J. Fluid Mech. (2007), *vol.* 574, *pp.* 169–178.
doi:10.1017/S0022112006004058 Printed in the United Kingdom

On the inversion of the von Kármán street in the wake of a confined square cylinder

SIMONE CAMARRI[1] AND FLAVIO GIANNETTI[2]

[1]Dipartimento di Ingegneria Aerospaziale, Università di Pisa, Italy
[2]Dipartimento di Ingegneria Meccanica, Università di Salerno, Italy

(Received 5 September 2006 and in revised form 15 November 2006)

This paper considers the incompressible two-dimensional laminar flow around a square cylinder symmetrically positioned in a channel. In this type of flow, even if vortices of opposite sign are alternately shed from the body into the wake as in the unconfined case, an inversion of their position with respect to the flow symmetry line takes place further downstream. A numerical analysis is carried out to investigate the physical origin of this phenomenon and to characterize the position in the wake at which the vortices cross the symmetry line. It is shown that, for low to moderate blockage ratios, the fundamental cause of the inversion of the vortices is the amount of vorticity present in the incoming flow, and a dynamic interpretation in terms of vorticity interference in the wake is given. Further insight is gained through a linear stability analysis of the vortex shedding instability.

1. Introduction

The flow around a cylinder confined in a channel is of interest in many applications, such as the design of vortex meters, in which the flow velocity is indirectly obtained by measuring the vortex-shedding frequency. In some applications a cylinder is introduced into a channel flow to enhance mixing and heat transfer. Owing to its practical interest, this configuration, which is characterized by the blockage ratio β, i.e. the ratio between the length of the cylinder sides and the channel height, has been widely studied in the literature. In the present study the laminar flow around a symmetrically confined square cylinder is considered, which has been studied in many works; for instance, both experimental and numerical results are reported in Davis, Moore & Purtell (1984) for $\beta = 1/4$ and $1/6$, and in Suzuki *et al.* (1993) and Suzuki & Suzuki (1994) for $1/20 \leqslant \beta \leqslant 1/2$. Numerical simulations are documented in Bernsdorf *et al.* (1998), Breuer *et al.* (2000) and Guo *et al.* (2003) for $\beta = 1/8$ and in Turki, Abbassi & Nasrallah (2003) for $\beta = 1/8$, $1/6$ and $1/4$. A detailed analysis of the time-averaged momentum equation is given in Saha, Muralidhar & Biswas (2000) for $\beta = 1/10$. Finally, several studies exist in which attention is also focused on heat transfer, such as Sharma & Eswaran (2005) and Rahnama & Hadi-Moghaddam (2005).

In the present study special attention is payed to a peculiar phenomenon that occurs in this type of flow, i.e. the inversion of the von Kármán street in the wake. More precisely, vortices are alternately shed in the wake as in the unconfined case, i.e. if the flow is from left to right, clockwise and counterclockwise vortices are shed from the upper and lower sides of the cylinder, respectively. However, at a certain distance along the wake, depending on both the Reynolds number and the blockage ratio β, the trajectories of the two families of vortices intersect and, further downstream,

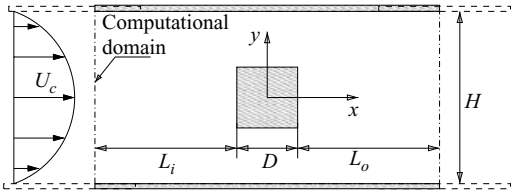

FIGURE 1. Flow configuration, frame of reference and computational domain (not in scale).

their position with respect to the symmetry line is inverted, i.e. counterclockwise and clockwise vortices are positioned in the upper and lower half of the wake, respectively. Experimental evidence of the inversion of the von Kármán street is available both for laminar (Davis *et al.* 1984; Suzuki *et al.* 1993) and turbulent flow (Yao, Nakatani & Suzuki 1995). This phenomenon also occurs for circular cylinders, as shown, for instance, in Sahin & Owens (2004) and in Zovatto & Pedrizzetti (2001).

To our knowledge, the inversion of the von Kármán street has been studied in detail only in Suzuki *et al.* (1993) and Suzuki & Suzuki (1994), in which it is argued that the inversion occurs only for $\beta \geqslant 0.1$ and is essentially caused by the effect of the lift-up of the vorticity layers that are adjacent to the confining walls. Note that Suzuki & Suzuki (1994) consider a configuration with a high blockage ratio ($\beta = 0.3$); in this case a strong interaction exists between the wake and the confining walls.

The aim of the present paper is to investigate in greater detail the inversion of the von Kármán street for moderate values of the blockage ratio ($1/10 \leqslant \beta \leqslant 1/6$), in which the interaction between the wake and the flow near the confining walls is weaker than in the case considered in Suzuki & Suzuki (1994). Numerical simulations have been carried out in order to identify which of the following factors play a leading role in the inversion: (i) the confinement, (ii) the vorticity generated by the confining walls and (iii) the shape of the incoming flow. The inversion of the wake vortices is also studied here through a linear stability analysis of the flow.

2. Flow configuration, numerical tools and validation

The incompressible flow over an infinitely long square cylinder symmetrically confined by two parallel planes is considered. Far upstream, the incoming flow is assumed to have a Poiseuille profile with maximum centreline velocity U_c. Figure 1 shows the geometry, the frame of reference and the notation. Values of the Reynolds number $Re = DU_c/\nu$ and of the blockage ratio $\beta = D/H$ are considered for which (*a*) vortex shedding is present, (*b*) the flow is two-dimensional and (*c*) the incoming Poiseuille flow is stable (roughly, $Re_H = U_c H/\nu \leqslant 2000$). The first requirement imposes a lower bound on Re, Re_{cr}, which is a function of β (see, for instance, Sharma & Eswaran 2005 and Breuer *et al.* 2000). Conversely, the stability of the incoming Poiseuille flow imposes an upper bound on Re, which is an increasing function of β: $Re = (U_c H/\nu)\beta \leqslant 2000\beta$. Thus, vortex shedding with a stable incoming flow is possible only if $Re_{cr} < 2000\beta$, which is satisfied only for approximately $\beta > 1/40$ if we assume that, for low values of β, Re_{cr} approaches the critical value found in the unconfined case, $Re_{cr} \simeq 54$ (see Kelkar & Patankar 1992). The same behaviour of Re_{cr} as β tends to zero has been observed in the case of circular cylinders (see Sahin & Owens 2004). Finally, the flow is two-dimensional when Re is lower than an upper bound, whose value has not been systematically studied in the literature, but may safely be assumed to be at least equal to the one found in the unconfined case

Grid	L_i/D	L_o/D	β	N_x	N_y	Spacing	N_e	Min./Max. Δ_x	Min./Max. Δ_y
UG	12	51	1/8	1024	128	uniform	16	0.0625/0.0625	0.0625/0.0625
SG8	12	35	1/8	660	260	stretched	90	0.010/0.165	0.012/0.107
SG6	12	35	1/6	660	260	stretched	90	0.010/0.165	0.012/0.068
SG10	12	35	1/10	660	284	stretched	90	0.010/0.165	0.012/0.116

TABLE 1. The computational domains and grids; for L_i and L_o see figure 1; N_x and N_y are the number of discretization points in the x- and y-directions, respectively; N_e is the number of nodes on each edge of the cylinder; Δ_x and Δ_y are the discretization sizes in the x- and y-directions, respectively.

($Re \simeq 161$, Robichaux, Balachandar & Vanka 1999). The blockage ratio is expected to have a stabilizing effect on three-dimensional instabilities.

The incompressible and two-dimensional Navier–Stokes equations for Newtonian fluids, written in conservative form, are discretized in space on a staggered Cartesian mesh by a standard centred and second-order-accurate finite-difference scheme. A parabolic velocity profile is imposed at the inflow boundary and no-slip and convective boundary conditions are applied on the confining walls and on the outflow boundary, respectively. A few additional simulations are also carried out using a different inlet profile and/or by imposing symmetry boundary conditions on the confining walls. The presence of the cylinder is simulated by an immersed-boundary technique that preserves second-order accuracy. Finally, the resulting semi-discrete equations are advanced in time by a mixed Crank–Nicholson/Adams–Bashforth scheme, in which the diffusive terms and the pressure field are treated implicitly and the convective terms explicitly. Thus, a linear system is solved at each time iteration by an LU factorization of the system matrix.

A linear temporal stability analysis has also been carried out on both the steady and time-averaged flow fields to gain a deeper comprehension of the inversion process. For this, the flow is decomposed into a base flow and a small-amplitude disturbance, which depends exponentially on time. The linearized equations for the disturbance are discretized in space with the same finite-difference scheme adopted for the temporal simulations, and the resulting generalized eigenvalue problem is solved with an inverse iteration algorithm. Further details on the numerical schemes and the stability analysis can be found in Camarri & Giannetti (2006) and Giannetti & Luchini (2007).

Two grids were used for the case $\beta = 1/8$, namely a uniform one (UG) and a stretched one (SG8), whereas two stretched grids have been used for $\beta = 1/6$ and $1/10$; more details are given in table 1. The stretched grids allow a finer grid resolution near the cylinder and are built as described in Camarri & Giannetti (2006). For the temporal discretization, a non-dimensional time step $\Delta T\ U_c/D$ equal to 5×10^{-3} has been used on the stretched grids and one equal to 2.5×10^{-2} on the uniform grid.

Preliminary simulations of the case $\beta = 1/8$ have been carried out to check the grid convergence of the results and the sensitivity to the dimensions of the computational domain. The value of the simulated vortex-shedding frequency has been monitored, as it is a sensitive parameter and a good indicator of the simulation quality, as confirmed for instance in Turki *et al.* (2003) and in Breuer *et al.* (2000). The shedding frequency f is given in terms of the Strouhal number St ($St = f\ D/U_c$). It was found that on grid SG8 St changes only at the 5th decimal unit when L_i/D is halved or when L_o/D is reduced by 25%. To check grid convergence, a set of simulations with increasing spatial resolution was carried out on the computational domain of grid SG8 at the

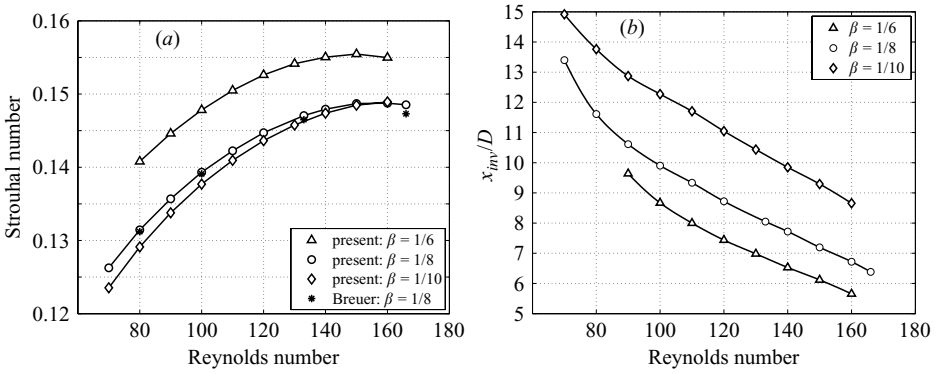

FIGURE 2. (*a*) Strouhal number vs. Reynolds number obtained on grid SG8 at different blockage ratios, together with results from Breuer *et al.* (2000). (*b*) *x*-coordinate (x_{inv}/D) of the intersection point of the vortex trajectories vs. Reynolds number.

highest Reynolds number considered here, $Re = 166$. The starting resolution, 204×74, was progressively increased by a factor approximately equal to 1.35 in each spatial direction. Besides St, the x-coordinate, x_{inv}, at which the trajectories of the wake vortices intersect the line $y = 0$ was monitored (details are given in § 3). The tests showed that convergence of the results was obtained on SG8, and a further increase in spatial resolution up to 800×300 involved variations of the Strouhal number as low as 0.2% and of x_{inv} of about 0.9% ($\Delta x_{inv} < 0.06D$). At $Re = 90$, St obtained with grid UG is only 1.6% higher than obtained with grid SG8 and x_{inv} is about 1.3% larger than in SG8, indicating that grid UG can be safely used up to this value of Re.

The numerical tools for the linear stability analysis were also validated by evaluating the critical Reynolds number for vortex shedding instability for $\beta = 1/8$ using grid UG. An unstable global mode was found at $Re_{cr} = 59$, which is in good agreement with the value $Re_{cr} \simeq 60$ found in Breuer *et al.* (2000). Also, the frequency of the linearly unstable mode, $St = 0.1196$, is in good agreement with the frequency of oscillation of the wake, $St = 0.1198$, found by numerical simulation at $Re = 60$ in Breuer *et al.* (2000).

3. Results and discussion

In figure 2(*a*) the Strouhal number is plotted as a function of the Reynolds number obtained with the non-uniform grids for blockage ratios $\beta = 1/6$, $1/8$, and $1/10$. The results obtained in Breuer *et al.* (2000) for $\beta = 1/8$ using a finite volume method are also reported for validation; they are in good agreement with those obtained here, the maximum difference in St being approximately 0.8% at $Re = 166$. In agreement with the findings of Turki *et al.* (2003), St increases with increasing β, while the shape of the St vs. Re curve does not significantly change with β.

In figure 3(*a*) an instantaneous vorticity field, obtained for $\beta = 1/8$ with grid SG8, is plotted together with the trajectories of the wake vortices and some profiles of the time-averaged streamwise velocity. The trajectories of the vortices are obtained by following the local minima of pressure in time. Figure 3(*a*) shows that vortices are shed from the cylinder as in the unconfined case, i.e. negative vortices (dark grey) from the top and positive (light grey) from the bottom, but at about 10 diameters behind the cylinder the trajectories of the positive and negative vortices cross the

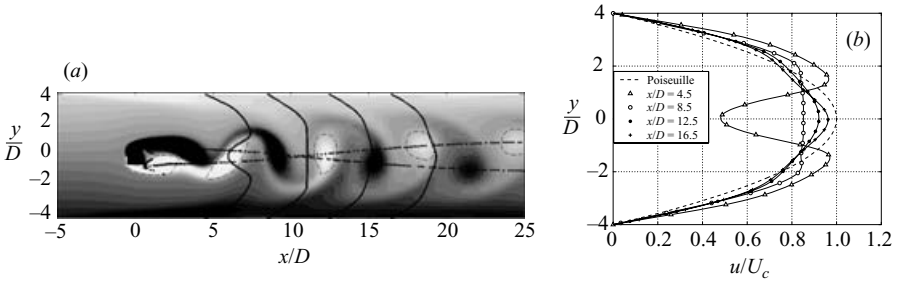

FIGURE 3. Grid SG8, $\beta = 1/8$, $Re = 90$: (*a*) trajectory of the wake vortices, identified by the criterion given in Hunt, Wray & Moin (1988) and shown by a dashed line. The vorticity, made non-dimensional by D and U_c, ranges from -0.8 (dark grey) to $+0.8$ (white). (*b*) Some profiles of the time-averaged streamwise velocity as sketched along the wake in (*a*).

symmetry plane $y = 0$ and their positions become inverted, i.e. the positive vortices stay in the $y > 0$ region and the negative ones in $y < 0$. The x-section at which the vortex trajectories intersect (x_{inv}) has been determined and is plotted in figure 2(*b*) as a function of the Reynolds number. For each value of β, x_{inv} decreases monotonically with Re and the trend is almost linear when Re is larger than a threshold value, which seems to increase weakly with β. The value of x_{inv} decreases with increasing β and the three curves of figure 2(*b*) are almost parallel in the region of linearity. A possible interpretation of the monotone decrease of x_{inv} with Reynolds number is given in the following.

The flow around a cylinder confined in a channel differs from the unconfined case with uniform free-stream velocity mainly in three factors: (*a*) the vorticity of the incoming flow, (*b*) the confinement effect and (*c*) the production of new vorticity due to the no-slip boundary conditions on the confining walls. Some simulations have therefore been carried out on grid UG with the objective of isolating the effects of each factor on the inversion of the von Kármán street.

In order to keep only the effect of confinement, one simulation was carried out for $\beta = 1/8$ with constant inflow profile (no vorticity in the incoming flow) and symmetry boundary conditions on the confining walls. In this case the reference velocity is the constant inflow velocity and two Reynolds numbers have been simulated, $Re = 90$ and 160. As also confirmed by simulations of a similar configuration available in Suzuki *et al.* (1993), no inversion of the wake vortices was observed.

At a later stage, the effect of both flow confinement and the vorticity of the incoming flow were kept. This was done by imposing the Poiseuille profile at the inflow, as in the original case, and symmetry boundary conditions on the confining walls, thus interrupting the vorticity production mechanism mentioned above and avoiding the presence of an intense vorticity layer near the confining walls. These simulations were carried out at $Re = 90$ and 160. An instantaneous vorticity field obtained at $Re = 90$ is plotted in figure 4, where the inversion of the wake vortices can be observed, and a similar result is found for $Re = 160$. It may thus be deduced that, at least at the blockage ratio considered and in the range $90 \leqslant Re \leqslant 160$, the flow confinement and the free-stream vorticity are sufficient to cause the inversion of the von Kármán street. This might seem in contrast with the claim in Suzuki & Suzuki (1994) that the inversion of the von Kármán street is mainly caused by the vorticity layers on the sidewalls, which are reinforced by the production of new vorticity and lifted up from the walls. But it is important to point out that in Suzuki & Suzuki (1994) a blockage

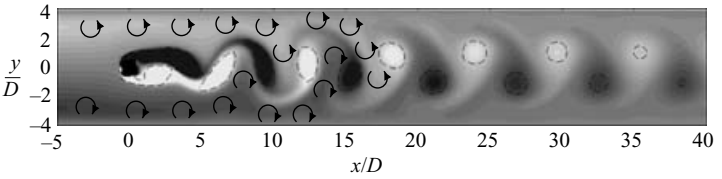

FIGURE 4. Grid UG, $Re = 90$, Poiseuille profile imposed at the inflow boundary, symmetry boundary conditions on the confining walls: detailed view of the wake vortices. The non-dimensional vorticity ranges from -0.5 (dark grey) to $+0.5$ (white).

ratio $\beta = 0.3$ is investigated, for which the interaction between the wake and the flow near the confining walls is more complex and important than in the present case. However, our computations show that the vorticity layer near the confining walls does not play a dominant role in the inversion of the von Kármán street at least for low values of the blockage ratio, while the fundamental mechanism is the entrainment of the vorticity of the incoming flow into the wake. The elimination of the no-slip boundary conditions on the sidewalls decreases the complexity of the flow in the wake and simplifies the interpretation of the phenomenon. The sign of the incoming-flow vorticity in figure 4 has been highlighted by arrows indicating the direction of rotation of the fluid particles. The free-stream vorticity is convected into the wake due to the velocity induced by the wake vortices and, in turn, induces a velocity in the wake vortices which tends to push them towards the inverted position that can be observed further downstream. The new vorticity that is generated near the confining walls in the original flow (when no-slip boundary conditions are applied) reinforces this mechanism, because it has the same sign as the vorticity of the incoming flow, i.e. positive for $y > 0$ and negative for $y < 0$.

To confirm our interpretation of figure 4, further tests were carried out in which symmetry boundary conditions are again imposed on the confining walls and the Poiseuille flow is substituted by a piecewise-constant velocity profile. As sketched in figure 5, the new profile is symmetrical with respect to $y = 0$, where the velocity is maximum, and has two discontinuities at $y/D = \pm 2.667$. On each side ($y > 0$ and $y < 0$), the location of the vorticity sheet is chosen to coincide with the centre of gravity of the vorticity distribution of the original Poiseuille profile. The new profile has the same mass flow rate as the Poiseuille one, and the mean velocity over the channel height U_m is now the reference velocity for the tests, which have been carried out at $Re_m = U_m\ D/\nu = 90$. The variation of the velocity Δu at the discontinuity is directly proportional to the intensity of the vorticity sheets, and four simulations have been carried out, with $\Delta u = 0.1,\ 0.2,\ 0.3,\ 0.4$. As in the case of the Poiseuille profile, positive vorticity is introduced for $y > 0$ and negative for $y < 0$. The resulting vorticity fields are shown in figure 5: consistently with our interpretation of the role of the incoming-flow vorticity, the vertical distance between the wake vortices decreases from $\Delta u = 0.1$ to 0.2, and inversion occurs when $\Delta u = 0.3$. When Δu is further increased to $\Delta u = 0.4$, inversion is anticipated and the vertical distance between the opposite vortices in the far wake is increased.

The dominant role played in the inversion by the incoming flow vorticity might also explain the monotone decrease of the inversion length x_{inv} as the Reynolds number is increased (see figure 2*b*). For fixed blockage ratio and fluid properties, the amount of vorticity of each sign contained in the undisturbed Poiseuille flow increases linearly with the flow Reynolds number (both being linearly proportional to the centreline

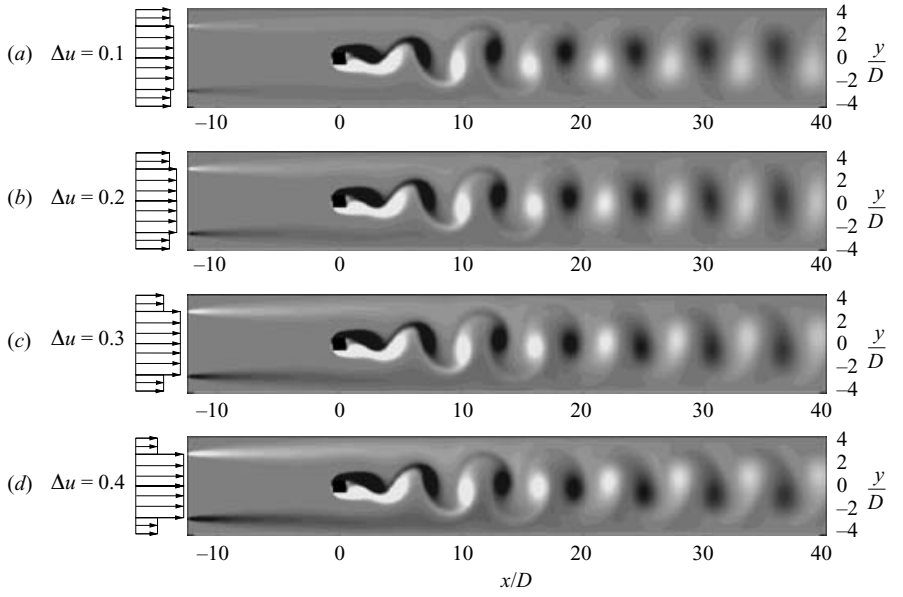

FIGURE 5. Grid UG, piecewise-constant inflow profile (qualitatively sketched on the left-hand side), symmetry boundary conditions on the confining walls, $Re = 90$: instantaneous vorticity fields obtained by varying the velocity discontinuity Δu in the inflow profile. Light and dark colours stand for positive and negative values, respectively.

velocity), and the effect on the inversion is then qualitatively the same as that observed in figure 5, where the incoming-flow vorticity was controlled artificially.

Returning to the original flow, figure 3(*b*), plotting time-averaged streamwise velocity profiles at different x-sections, shows that the velocity defect in the wake disappears after the inversion of the von Kármán street. The velocity induced on the centreline by a street with negative vortices in the upper part (as in the unconfined wakes) is directed upwind and, therefore, generates a velocity defect in the mean profile, while the opposite happens when the von Kármán street is inverted, as shown in figure 3(*a*). Note that the disappearance of the velocity defect at a finite distance from the cylinder is a fundamental difference with the unconfined case, where it happens only asymptotically far from the cylinder.

To further investigate the connection between the velocity defect and the inversion of the wake vortices, a linear stability analysis of the flow has been carried out at $Re = 90$ (grid UG), taking as the base flow the time-averaged flow field obtained from the temporal simulation, where the wake defect is recovered at $x_{inv} \simeq 10$ (see figure 3*b*). Examples of such an analysis may be found in Monkewitz, Huerre & Chomaz (1993) and Hammond & Redekopp (1997). Using the time-averaged flow as the base flow retains some nonlinearity in the stability analysis, a significant feature in our case, where the recovery of the velocity defect in the wake is strongly enhanced by the von Kármán street. An unstable linear mode is found, whose frequency ($St = 0.1368$) is almost identical to that of vortex shedding in the simulation ($St = 0.137$). This mode was superposed on the time-averaged flow and it was verified that in the resulting field wake vortices are present, and they cross the centreline approximately where the velocity defect of the wake disappears, i.e. at a position independent of the relative weight by which the linearly unstable mode is added to the base

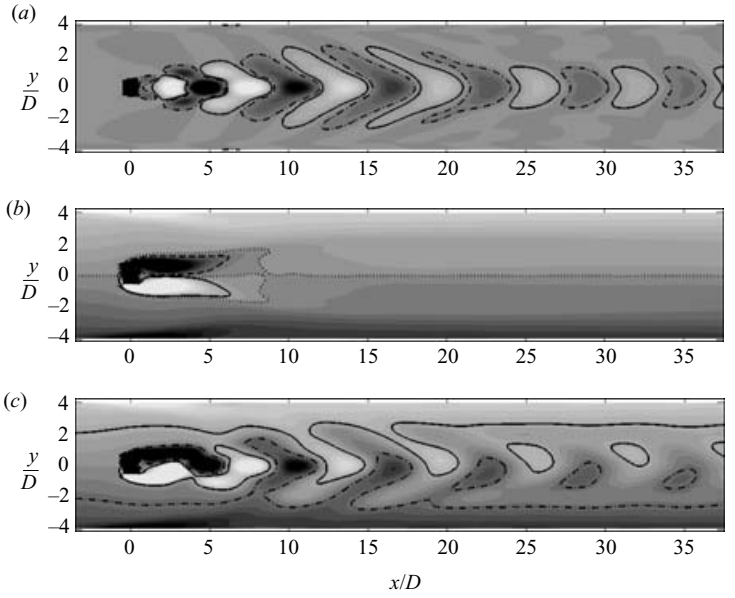

FIGURE 6. Blockage ratio $\beta = 1/8$, $Re = 90$: vorticity of (*a*) the linearly unstable mode, (*b*) the time-averaged flow field and (*c*) superposition of (*a*) and (*b*). Light (continuous isocontours) and dark colours (dashed isocontours) stand for positive and negative values, respectively. The dotted line in (*b*) is the isocontour of the zero value.

flow (see figure 6, where the unstable mode, the averaged flow field and their sum are plotted). The vorticity of the unstable mode and of the averaged flow field is symmetrical and antisymmetrical, respectively, with reference to the centreline $y = 0$, as in the unconfined case. However, unlike the unconfined case, the disappearance of the wake defect implies a change in the vorticity sign of the base flow moving downstream near the centreline, as can be deduced from figure 6(*b*). Thus, in the sum of fields (*a*) (symmetrical) and (*b*) (antisymmetrical), the sign of the vortices near $y = 0$ must change in crossing the point where the wake defect disappears, since, at that point, field (*a*) is unchanged and symmetrical, while the sign of (*b*) is reversed.

The same qualitative behaviour is observed when the stability analysis is carried out taking as the base flow the steady solution of the Navier–Stokes equations, found numerically by the Newton–Raphson method, at Reynolds numbers for which the vortex shedding instability would be present. In this case, however, the disappearance of the velocity defect in the base flow takes place at a distance which is larger than in the time-averaged flow field, and which decreases as β is increased. In particular, while for $\beta = 1/8$ the disappearance of the velocity defect was not observed on UG, for $\beta = 1/2$ it is found at about $x \simeq 12D$.

These results suggest the existence of a correlation between velocity defect in the wake and inversion. It is then reasonable to expect that the von Kármán street should invert approximately where the velocity defect disappears, provided the vortices are still sufficiently strong. If this holds, since it can be shown that in stable channel flow the Poiseuille profile is recovered at a finite distance behind the cylinder, the inversion should also be observed for low values of β. This is in contrast to Suzuki *et al.* (1993), where the inversion was not observed when $\beta < 0.1$. In particular, they simulated the case $\beta = 0.05$ with a very large computational domain, i.e. $L_i = 39.5D$ and $L_o = 199.5D$, but with a very coarse grid. Although clustered around the cylinder, they

used only 207 and 54 nodes in the x- and y-directions, giving an average resolution $\Delta_x \simeq 1.15D$ and $\Delta_y \simeq 0.37$. In our opinion, the coarseness of the grid, together with the use of an upwind scheme (QUICK), might have anticipated the diffusion of the wake vortices before it was possible to observe their inversion, as confirmed by figure 8 (Case H) of Suzuki *et al.* (1993), where the instantaneous vorticity field obtained for $Re = 75$ and $\beta = 0.05$ is shown, and from which it is clear that the simulated wake vortices are completely diffused at about 50 diameters behind the cylinder. The same configuration was simulated here in a domain of size $L_i = 12D$ and $L_o = 115.5D$ with a uniform discretization $\Delta_x = \Delta_y = 1/8$, for $Re = 75$, identical to that in Suzuki *et al.* (1993), and $Re = 90$. In both cases, inversion of the von Kármán street was observed about 70 diameters behind the cylinder (not shown here for brevity).

4. Conclusions

The inversion of the von Kármán street in the laminar wake of a symmetrically confined square cylinder has been studied. Low blockage ratios were considered ($1/10 \leqslant \beta \leqslant 1/6$), in order to concentrate on cases with a weak interaction between the wake and the flow close to the confining walls.

The results of this analysis showed that the distance from the cylinder at which the von Kármán street inverts (x_{inv}) decreases monotonically when either Re or β are increased, and that the decrease of x_{inv} is linear with respect to Re when $Re >\sim 110$.

A set of *ad-hoc* simulations demonstrated that the blockage effect alone is not sufficient to produce the inversion of the wake street. Conversely, the vorticity of the incoming flow is of fundamental importance for the inversion since, together with the blockage effect due to the confining walls, it is sufficient to invert the wake. As a further confirmation of this, a set of simulations was carried out in which an artificial inflow condition allowed direct control of the vorticity introduced into the flow. The results showed that the wake inversion depends on the amount of vorticity introduced into the flow and that the inversion length decreases as the amount of incoming-flow vorticity is increased.

It was also pointed out that a significant difference between the flow considered and the unconfined case is related to the velocity defect in the wake: while in the unconfined case this defect disappears only asymptotically far from the cylinder, in the present case this happens at a finite distance, near the point at which the inversion of the von Kármán street occurs. The close correlation between the disappearance of the velocity defect in the wake and the inversion of the von Kármán street has been further demonstrated by a linear stability analysis of the vortex-shedding instability. As a result of this interpretation, since in the stable channel flow the velocity defect always disappears at a finite distance from the cylinder, it is reasonable to expect the inversion of the vortex street to occur also for low values of β. This has been proved to hold at least for $\beta = 1/20$, where the inversion of the von Kármán street was observed about 70 diameters behind the cylinder. A detailed analysis of the time-averaged momentum balance, as in Saha *et al.* (2000), might prove helpful in devising models to predict the inversion length, by monitoring, for instance, the leading terms that determine the convexity of the mean streamwise profile on the symmetry line.

Finally, there is no experimental campaign entirely devoted to investigating and quantifying the inversion of the von Kármán street in the flow considered here in the literature, only a few qualitative visualizations being reported. This would provide a necessary validation of, and support for, the present analysis, and help to explain this interesting phenomenon.

The authors are grateful to Professors G. Buresti, P. Luchini and M. V. Salvetti for their scientific support to the present work, and to Professor M. Breuer for providing his data. Part of the simulations were carried out thanks to the computational resources of DIMEC (Salerno) and of MAB (Bordeaux).

REFERENCES

Bernsdorf, J., Zeiser, T. H., Brenner, G. & Durst, F. 1998 Simulation of a 2D channel flow around a square obstacle with lattice-Boltzmann(BGK) automata. *Intl J. Mod. Phys.* C **9** (8), 1129–1141.

Breuer, M., Bernsdorf, J., Zeiser, T. & Durst, F. 2000 Accurate computations of the laminar flow past a square cylinder based on two different methods: lattice-Boltzmann and finite-volume. *Intl J. Heat Fluid Flow* **21**, 186–196.

Camarri, S. & Giannetti, F. 2006 Analysis of the wake dynamics of a confined square cylinder. *Tech. Rep.* ADIA 2006-2. Dipartimento di Ingegneria Aerospaziale, Univ. di Pisa.

Davis, R. W., Moore, E. F. & Purtell, L. P. 1984 A numerical-experimental study of confined flow around rectangular cylinders. *Phys. Fluids* **27**, 46–59.

Giannetti, F. & Luchini, P. 2007 Structural sensitivity of the cylinder wake's first instability *J. Fluid Mech.* (to appear).

Guo, W. B., Wang, N. C., Shi, B. C. & Guo, Z. L. 2003 Lattice-BGK simulation of a two-dimensional channel flow around a square cylinder. *Chinese Phys.* **12**, 67–74.

Hammond, D. & Redekopp, L. 1997 Global dynamics of symmetric and asymmetric wakes. *J. Fluid Mech.* **331**, 231–260.

Hunt, J. C. R., Wray, A. A. & Moin, P. 1988 Eddies, stream, and convergence zones in turbulent flows. *Tech. Rep.* CTR-S88. Center for Turbulence Research, Stanford University.

Kelkar, K. M. & Patankar, S. V. 1992 Numerical prediction of vortex shedding behind square cylinders. *Intl J. Numer. Methods Fluids* **14**, 327–341.

Monkewitz, P. A., Huerre, P. & Chomaz, J. M. 1993 Global linear stability analysis of weakly non-parallel shear flows. *J. Fluid Mech.* **251**, 1–20.

Rahnama, M. & Hadi-Moghaddam, H. 2005 Numerical investigation of convective heat transfer in unsteady laminar flow over a square cylinder in a channel. *Heat Transfer Engng* **26** (10), 21–29.

Robichaux, J., Balachandar, J. & Vanka, S. P. 1999 Three-dimensional Floquet instability of the wake of square cylinder. *Phys. Fluids* **11**, 560–578.

Saha, A. K., Muralidhar, K. & Biswas, G. 2000 Vortex structures and kinetic energy budget in two-dimensional flow past a square cylinder. *Comp. Fluids* **29**, 669–694.

Sahin, M. & Owens, R. G. 2004 A numerical investigation of wall effects up to high blockage ratios on two-dimensional flow past a confined circular cylinder. *Phys. Fluids* **16**, 1305–1320.

Sharma, A. & Eswaran, V. 2005 Effect of channel confinement on the two-dimensional laminar flow and heat transfer across a square cylinder. *Numer. Heat Transfer* A **47**, 79–107.

Suzuki, H., Inoue, Y., Nishimura, T., Fukutani, K. & Suzuki, K. 1993 Unsteady flow in a channel obstructed by a square rod (crisscross motion of vortex). *Intl J. Heat Fluid Flow* **14**, 2–9.

Suzuki, K. & Suzuki, H. 1994 Instantaneous structure and statical feature of unsteady flow in a channel obstructed by a square rod. *Intl J. Heat Fluid Flow* **15**, 426–437.

Turki, S., Abbassi, H. & Nasrallah, S. B. 2003 Effect of the blockage ratio on the flow in a channel with built-in square cylinder. *Comput. Mech.* **33**, 22–29.

Yao, M., Nakatani, M. & Suzuki, K. 1995 Flow visualization and heat transfer experiments in a turbulent channel flow obstructed with an inserted square rod. *Intl J. Heat Fluid Flow* **16**, 389–397.

Zovatto, L. & Pedrizzetti, G. 2001 Flow about a circular cylinder between parallel walls. *J. Fluid Mech.* **440**, 1–25.